Supplementary Materials for

Switchable third $ScFeO_3$ polar ferromagnet with $YMnO_3$-type structure

Yosuke Hamasaki[1], Tsukasa Katayama[2], Shintaro Yasui[3], Takahisa Shiraishi[4], Akihiro Akama[4], Takanori Kiguchi[4], Tomoyasu Taniyama[3], and Mitsuru Itoh[3]

[1]Department of Applied Physics, National Defense Academy, Yokosuka 239-8686, Japan

[2]Department of Chemistry, The University of Tokyo, Bunkyo-ku, Tokyo 112-0033, Japan

[3]Laboratory for Materials and Structures, Tokyo Institute of Technology, 4259-J2-19, Nagatsuta-cho, Midori-ku, Yokohama 226-8503, Japan

[4]Institute for Materials Research, Tohoku University, 2-1-1 Katahira, Aoba-ku, Sendai 980-8577, Japan

The PDF file includes

Materials and Methods
Figures S1 to S8

Materials and Methods

Materials

$ScFeO_3$ films were deposited by pulsed laser deposition (PLD) technique with the fourth-harmonic wave of a Nd:YAG laser (λ = 266 nm). $La_{1-x}Sr_xMnO_3$ (*x*LSMO) (*x*= 0.2 and 0.3) films were grown on $SrTiO_3$(STO)(111) substrate at 700°C under O_2 pressure of 20 mTorr. $ScFeO_3$ films were deposited at 700°C under O_2 pressure of 20 mTorr. Thickness of *x*LSMO films were ~100 nm, and that of $ScFeO_3$ film was ~50 nm. The repetition rate and fluence of the laser were 5 Hz and 0.96 Jcm^{-2}, respectively. A $ScFeO_3$ target was prepared using α-Fe_2O_3 and Sc_2O_3 powders, and sintering at 1350 °C for 6 hours in air. *x*LSMO targets were prepared using La_2O_3, $SrCO_3$ and MnO_2 powders. The mixtures were sintered at 1450°C for 12h under O_2 flow.

Methods

Structural characterization

The crystal structures of the films were characterized by high-resolution X-ray diffraction (HRXRD) using a Rigaku Smart-Lab diffractometer, where X-ray was monochromatized using a Ge(220) 2-bounce crystal and Cu Kα radiation (λ=1.5406 Å). Reciprocal space mapping (RSM) was performed to determine the lattice constants. The film structure was characterized by high-angle annular dark-field scanning transmission electron microscopy (HAADF-STEM) and energy dispersive X-ray (EDX) observations using a JEOL JEM-ARM200F.

Ferroelectric and magnetic characterization

In order to evaluate the ferroelectric properties, we fabricated a capacitor structure. Pt with ϕ100 μm and 0.2LSMO film, used for top and bottom electrodes, respectively, were deposited on $SrTiO_3$(111) substrates. Polarization *vs.* electric field (*P*-*E*) hysteresis loops were collected using a ferroelectric tester (Radiant, Precision Multiferroic II and Toyo Corporation, FCE). Field-cooled (FC)

dc magnetizations and magnetization hysteresis curves were measured using a Quantum Design Magnetic Property Measurement System (MPMS). FC magnetizations were recorded at 1000 Oe in the temperature range 5-300 K. X-ray absorption spectroscopy (XAS) and X-ray magnetic circular dichroism (XMCD) spectra were measured at 35 K at a field of 1 kOe with polarized light switching mode after application of 50 kOe using BL16A in KEK-PF.

Detail of Deposition of $YMnO_3$-type $ScFeO_3$ on electrode film

In our previous work, single phase hexagonal $ScFeO_3$ films were obtained on $MgAl_2O_4(001)$ and $Al_2O_3(0001)$ substrates.[1] Based on the results, we selected candidates for bottom electrodes to stabilize $YMnO_3$-type $ScFeO_3$. First, we focused on a $MgAl_2O_4(001)$ substrate. $MgAl_2O_4$ have a spinel-type structure, and their in-plane symmetry is square. Conductive materials with spinel related structure are Fe_3O_4, $LiTi_2O_4$ and TiN, however these compounds are not suitable for a growth condition in an oxygen atmosphere. Then, we selected La doped $BaSnO_3$ with a perovskite structure. Lattice constants of $BaSnO_3$ is a = 4.1085 Å which is close that of $MgAl_2O_4$ (a = 4.042 Å). We attempted to grow $ScFeO_3$ films on La doped $BaSnO_3$ epitaxial films deposited on $SrTiO_3(001)$ substrates. Bixbyite-type $ScFeO_3$ was mainly grown, while $YMnO_3$-type $ScFeO_3$ was also grown as a secondary phase on $BaSnO_3$ film. Although we also attempted to deposit $ScFeO_3$ on the La doped $SrSnO_3$ film, the single phase of $YMnO_3$-type $ScFeO_3$ has not been obtained. Second, we focused on an $Al_2O_3(0001)$ substrate, whose structure is corundum-type with a hexagonal in-plane symmetry. Although we previously deposited $ScFeO_3$ film on films and substrates with hexagonal in-plane symmetry such as ZnO(0001), ITO(111) and Pt(111), $YMnO_3$-type $ScFeO_3$ could not be grown as a main phase. In the view point of lattice constants, in-pane lattice constant of $SrTiO_3(111)$ is close that of $Al_2O_3(0001)$. We attempted to grow $ScFeO_3$ film on conductive perovskite films ($SrRuO_3$, 0.3LSMO, and 0.2LSMO) on $SrTiO_3(111)$ substrate. As a result, we succeeded in

obtaining the $YMnO_3$-type $ScFeO_3$ film on the 0.2LSMO film on the $SrTiO_3(111)$ substrate.

Unit cell volume of *h*-$Lu_{1-x}Sc_xFeO_3$

The unit cell volume of *h*-$Lu_{1-x}Scx FeO_3$[2] and *h*-$ScFeO_3$ film (this work) was plotted in figure S1.

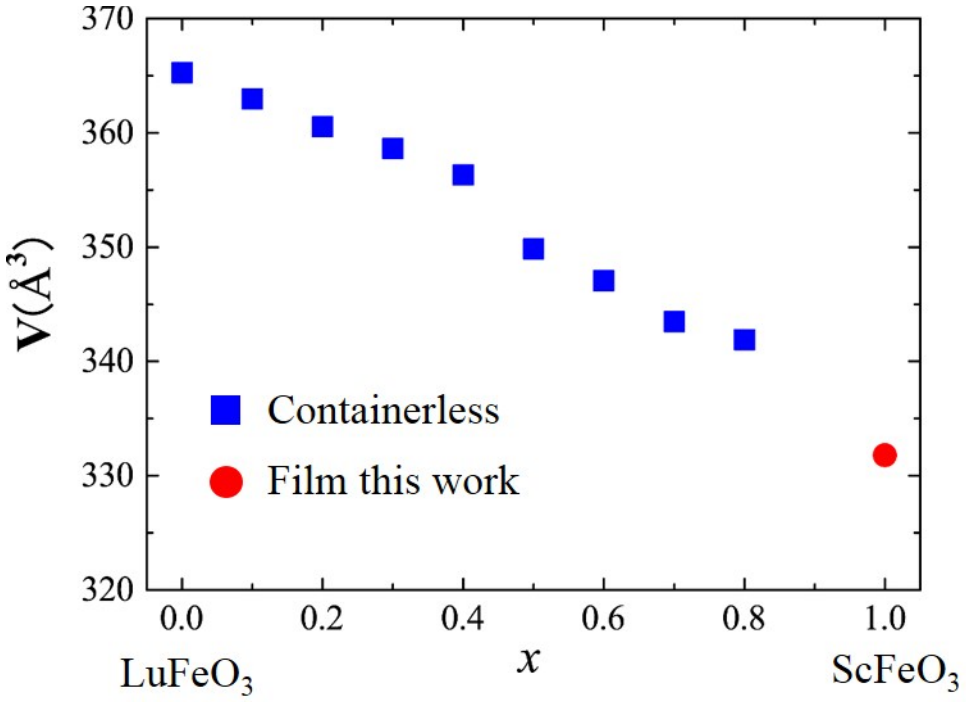

Figure S1. The unit cell volume of *h*-$Lu_{1-x}Sc_xFeO_3$. Blue squares and red circle correspond to cell volumes reported in ref. 2 and this work, respectively.

ϕ-scan of h-$Lu_{1-x}Sc_xFeO_3$

Figure S2 shows the ϕ-scan pattern recorded around the $ScFeO_3\{304\}$, $0.2LSMO\{110\}_{pc}$, and $STO\{110\}$ reflections. The ϕ-scans of the $0.2LSMO\{110\}_{pc}$ and $STO\{110\}$ reflections showed three peaks reflecting the in-plane three-fold symmetry. The peaks of $ScFeO_3\{304\}$ showed six-fold symmetry characterized by a hexagonal unit cell.

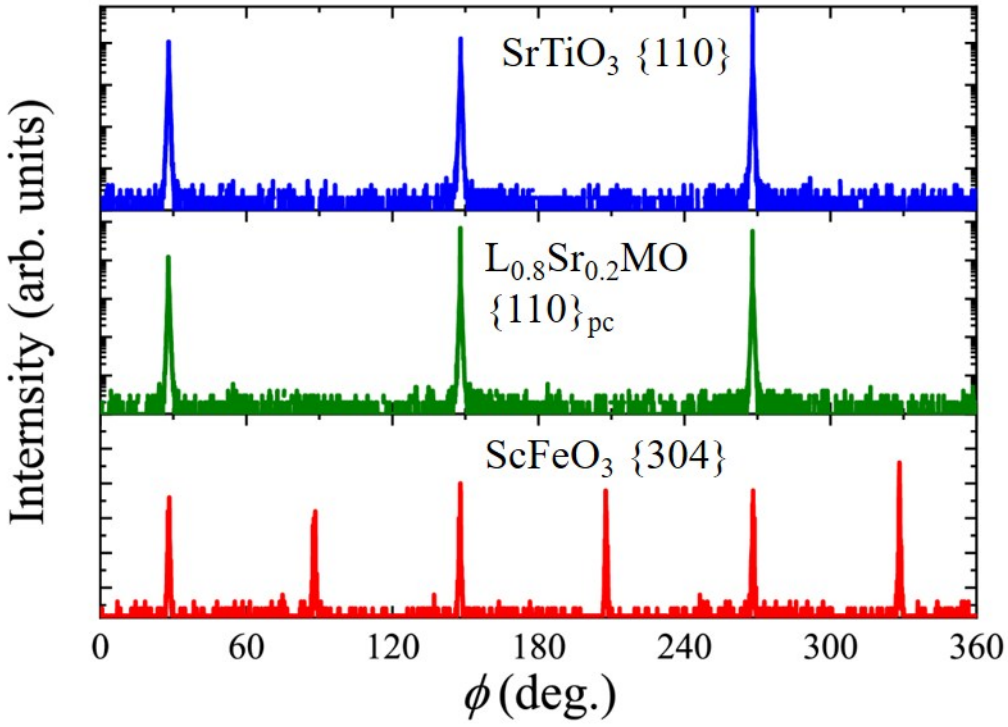

Figure S2. ϕ-scan patterns of $STO\{110\}$, $0.2LSMO\{110\}_{pc}$, and h-$ScFeO_3\{304\}$.

Crystal structure of corundum

Figure S3 shows a *P*-*E* hysteresis loop (red line) and *I*-*E*curve (black line) measured at 100 kHz and room temperature.

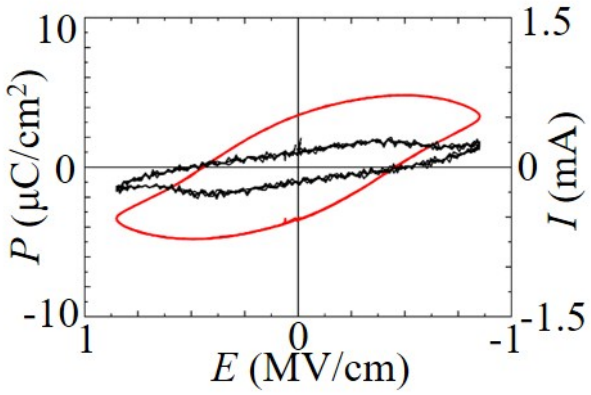

Figure S3. *P*-*E* hysteresis loop (red line) and *I*-*E*curve (black line) measured at 100 kHz and room temperature

Ferroelectric domain structure of *h*-$ScFeO_3$ film

The ferroelectric domain structure of the *h*-$ScFeO_3$ film was investigated by HAADF-STEM. Figure S4 shows the HAADF-STEM image around the ferroelectric 180° domain boundary in the $ScFeO_3$ film.

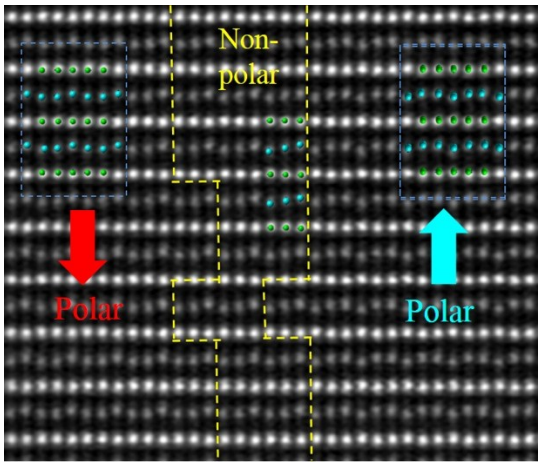

Figure S4. HAADF-STEM image around the ferroelectric 180° domain boundary in the $ScFeO_3$ film.

Characterization of the $InFeO_3$ film by XRD measurements

In order to distinguish between the polar (*P*6_3*cm*) and nonpolar (*P*6_3/*mmc*) structures, we performed HR XRD 2θ-ω scan along the $InFeO_3$ [-126] direction (*P*6_3/*mmc* notation), as shown in Figure S5. Figure S6 and S7 show HR XRD 2θ-ω patterns of *h*-$InFeO_3$ *-1/3 2/3 4* and *-2/3 4/3 8* reflections, respectively. Both peaks were not observed, indicating that the $InFeO_3$ film is a nonpolar *P*6_3/*mmc*.

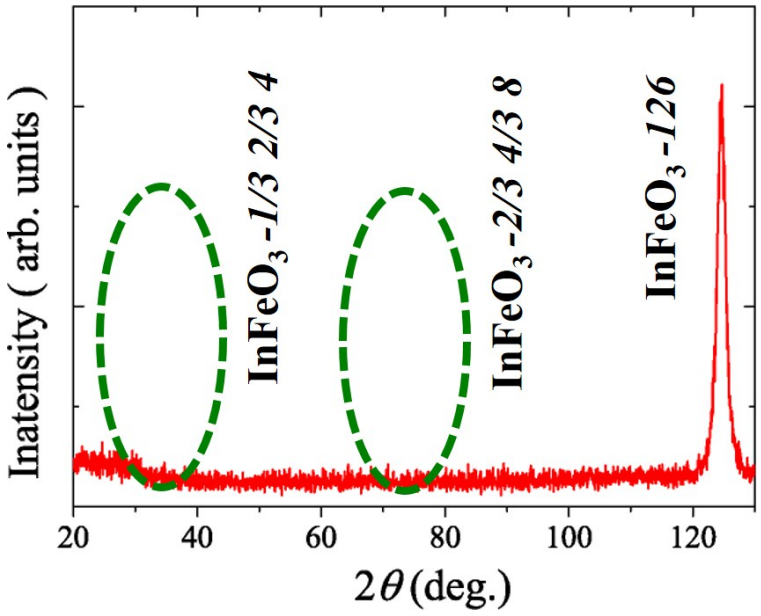

Figure S5 HR-XRD 2θ-ω pattern of the *h*-$InFeO_3$ film along *h*-$InFeO_3$ [-126] direction.

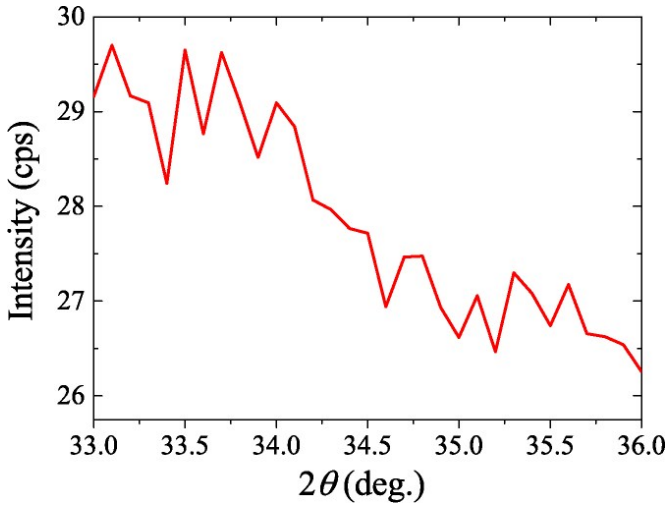

Figure S6. HR-XRD 2θ-ω pattern of the *h*-$InFeO_3$ film around *h*-$InFeO_3$ *-1/3 2/3 4* reflection.

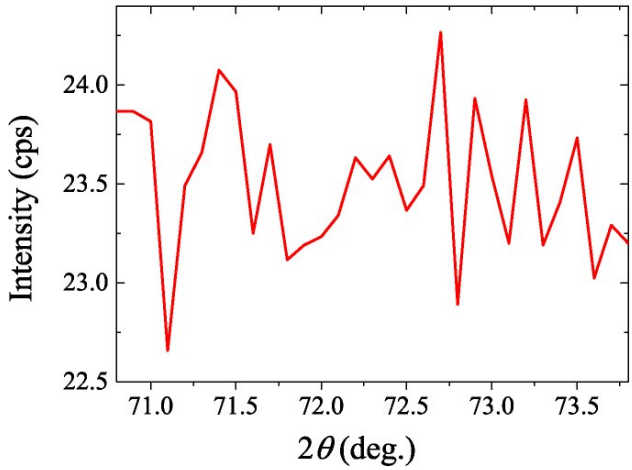

Figure S7. HR-XRD 2θ-ω pattern of the *h*-$InFeO_3$ film around *h*-$InFeO_3$ *-2/3 4/3 8* reflection.

<u>T_N vs lattice constant *c*</u>

Figure S8 shows T_N versus lattice constants *c* of *h*-*Re*FeO_3 and *h*-*Re*MnO_3, respectively. [2–7] Although the magnetic interaction along the *c*-axis is smaller than that along the *a*-axis, [8] T_N also decreases with the decrease in *c*. Compared with *Re*MnO_3, *Re*FeO_3 has a large *c*-axis length. This is because the occupancy of the d_{z2} orbital in *Re*FeO_3 yields a larger *c* lattice constant than does *Re*MnO_3, in which the d_{z2} orbital of Mn^{3+} is empty because of the repulsion between the electron and oxygen-anion ligands.

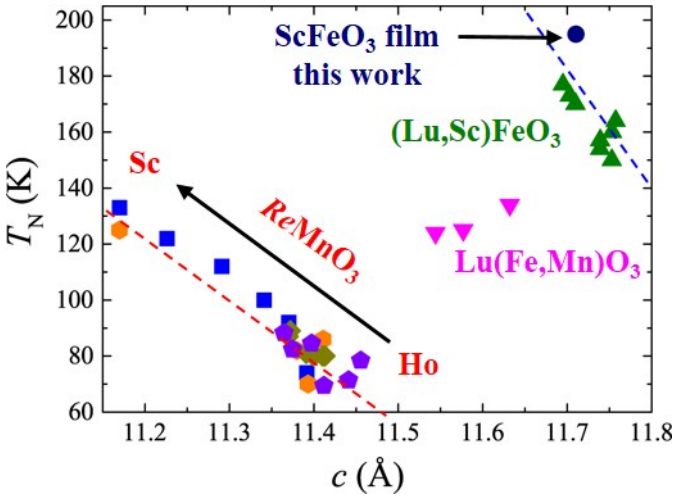

Figure S8 T_N vs. the lattice constant c of hexagonal *Re*FeO_3 and *Re*MnO_3.Green triangles, pink inverted triangles, ocher rhombus, orange hexagons, purple pentagons, and blue squares plot the results of Refs. 2, 3, 4, 5, 6, and 7. The navy blue circle corresponds to the $ScFeO_3$ film of this study. Dotted lines and solid lines are provided as guides.

REFERENCES

1 Y. Hamasaki, T. Shimizu, S. Yasui, T. Taniyama, O. Sakata and M. Itoh, *Cryst. Growth Des.*, 2016, **16**, 5214–5222.

2 A. Masuno, A. Ishimoto, C. Moriyoshi, H. Kawaji, Y. Kuroiwa and H. Inoue, *Inorg. Chem.*, 2015, **54**, 9432–9437.

3 S. M. Disseler, X. Luo, B. Gao, Y. S. Oh, R. Hu, Y. Wang, D. Quintana, A. Zhang, Q. Huang, J. Lau, R. Paul, J. W. Lynn, S.-W. Cheong and W. Ratcliff, *Phys. Rev. B*, 2015, **92**, 054435.

4 K. Uusi-Esko, J. Malm, N. Imamura, H. Yamauchi and M. Karppinen, *Mater. Chem. Phys.*, 2008, **112**, 1029–1034.

5 T. Katsufuji, S. Mori, M. Masaki, Y. Moritomo, N. Yamamoto and H. Takagi, *Phys. Rev. B*, 2001, **64**, 104419.

6 J. S. Zhou, J. B. Goodenough, J. M. Gallardo-Amores, E. Morán, M. A. Alario-Franco and R. Caudillo, *Phys. Rev. B - Condens. Matter Mater. Phys.*, 2006, **74**, 014422.

7 C. T. Wu, B. N. Lin and H. C. Ku, 2003, **41**, 652–661.

8 C. Xu, Y. Yang, S. Wang, W. Duan, B. Gu and L. Bellaiche, *Phys. Rev. B*, 2014, **89**, 205122.